

# Grid-Based Bayesian Filters With Functional Decomposition of Transient Density

Petr Tichavský , Senior Member, IEEE, Ondřej Straka , Member, IEEE,  
and Jindřich Duník , Senior Member, IEEE

**Abstract**—The paper deals with the state estimation of nonlinear stochastic dynamic systems with special attention to grid-based Bayesian filters such as the point-mass filter (PMF) and the marginal particle filter (mPF). In the paper, a novel functional decomposition of the transient density describing the system dynamics is proposed. The decomposition approximates the transient density in a closed region. It is based on a non-negative matrix/tensor factorization and separates the density into functions of the future and current states. Such decomposition facilitates a thrifty calculation of the convolution involving the density, which is a performance bottleneck of the standard PMF/mPF implementations. The estimate quality and computational costs can be efficiently controlled by choosing an appropriate decomposition rank. The performance of the PMF with the transient density decomposition is illustrated in a terrain-aided navigation scenario and a problem involving a univariate non-stationary growth model.

**Index Terms**—State estimation, nonlinear systems, nonlinear filtering, point-mass method, non-negative matrix factorization.

## I. INTRODUCTION

STATE estimation of nonlinear discrete-time stochastic dynamic systems from noisy measurements has been a subject of considerable research interest for many decades. It plays an indispensable role in fields such as navigation, speech and image processing, fault diagnosis, and adaptive control.

Within the Bayesian framework, a general solution to the state estimation problem is given by the Bayesian recursive relations (BRRs) inferring the probability density functions (PDFs) of the state conditioned on the measurements. The PDFs fully describe the immeasurable state of a possibly nonlinear or non-Gaussian stochastic dynamic system. The relations are analytically tractable for a limited set of models such as linear Gaussian models. In other cases, approximate solutions to the BRRs have to be employed, offering various approximation

levels. The Gaussian filters assuming the joint state and measurement prediction PDF being Gaussian are attractive for mildly nonlinear models, for which they offer computational efficiency with acceptable estimate quality. For strongly nonlinear or non-Gaussian models, one usually resorts to more complex (and thus computationally demanding) filters such as the particle filter (PF) [1], [2] or the point-mass filter (PMF) [3].

This paper considers the PMF [4], [5], [6] and the marginal PF (mPF) [7]. Both algorithms are based on a numerical solution to the BRRs. The PMF uses *deterministic* grid-based numerical integration rules and computes the conditional PDFs at the grid points only. The mPF approximates the conditional PDFs by empirical PDFs parametrized by a set of *random* grid points called samples and corresponding weights. For both PMF and mPF, a suitable specification of the number of grid points is critical as it affects the estimate accuracy and computational complexity. The predictive step is the computational bottleneck of the standard filter implementations, which limits the number of grid points from above. This step involves an evaluation of a convolution called the Chapman-Kolmogorov equation, where the grids for two consecutive time instants are combined through the transient PDF. The convolution complexity thus grows quadratically ( $\mathcal{O}(N^2)$ ) with the number of grid points  $N$ .

For the PMF, many techniques for computational complexity reduction were proposed, often with the price of extra approximations, the need for user-defined parameters, or only for particular models. The techniques are based on the following approaches:

- *Rao-Blackwellisation*: The techniques are designed for the conditionally linear models with Gaussian noises, where the expensive PMF estimates the nonlinearly modeled part of the state, whereas the remaining linearly modeled part is estimated by computationally cheap Kalman filters [8], [9], [10].
- *Separable prediction*: These techniques take advantage of an offline evaluation of the transient PDF, which is made possible by assuming a particular model and Gaussian noise. They do not use the convolution theorem, and the computational complexity depends on the state noise variance. In the worst-case scenario, it is still almost  $\mathcal{O}(N^2)$  [11].
- *Copula prediction*: Rather than the propagation of conditional PDFs, these techniques propagate the marginal PDFs and a copula, capturing the correlation. An optimal copula

Manuscript received 3 August 2022; revised 30 November 2022 and 19 January 2023; accepted 22 January 2023. Date of publication 2 February 2023; date of current version 8 February 2023. The associate editor coordinating the review of this manuscript and approving it for publication was Dr. Kunal Narayan Chaudhury. The work was supported by the Czech Science Foundation under Grant 22-11101S. (Corresponding author: Petr Tichavský.)

Petr Tichavský is with the Czech Academy of Sciences, Institute of Information Theory and Automation, 18208 Prague, Czech Republic (e-mail: tichavsk@utia.cas.cz).

Ondřej Straka and Jindřich Duník are with the Department of Cybernetics, University of West Bohemia, 30614 Pilsen, Czech Republic (e-mail: straka30@kky.zcu.cz; dunikj@kky.zcu.cz).

Digital Object Identifier 10.1109/TSP.2023.3240359

cannot generally be found; thus, its selection is a designer decision leading to an extra approximation error [12].

The PMF grid can also be designed using adaptive or sparse layouts [13]. Although such layouts lead to the reduction of the total number of the grid points, the order of the complexity is still  $\mathcal{O}(N^2)$ .

To reduce the computational complexity of the mPF, the algorithm proposed in [14] employs kernel density estimation while the paper [15] proposes an mPF algorithm with linear complexity by using the accept-reject technique.

In this paper, we propose handling the transient PDF in the form of its decomposition within a closed region. The decomposition is based on the non-negative matrix factorization<sup>1</sup> (NNMF) and symmetric NNMF [18]. The transient PDF is decomposed into a sum of products of functions of current and future states. The decomposition needs to be found once before the estimation itself and allows large grids to be handled while maintaining affordable computational complexity. A short version of this paper focused on the PMF only and decomposition for a scalar state only was presented in [19]. Application of the decomposition to the case with scalar state estimated by the mPF was treated in [20]. This paper provides an extension in the following directions:

- i) The decomposition is proposed for arbitrary state dimension. This includes a design of an efficient triangular lattice of function locations in the approximation region, different from the rectangular lattice proposed earlier.
- ii) The decomposition is also designed for heavy-tailed transient PDF, which appears in models involving outliers of the state.

The paper is organized as follows. Section II briefly summarizes elements of the PMF and mPF-based Bayesian state estimation. In Section III, the decomposition of the transient PDF is introduced and its calculation for multivariate Gaussian, univariate generalized Gaussian, and univariate Student-t distributed cases is demonstrated. The performance of the PMF with the proposed decomposition is studied in a terrain-aided navigation scenario and in a problem involving a univariate non-stationary growth modeling in Section IV. In Section V, the concluding remarks are drawn.

## II. GRID-BASED BAYESIAN FILTERS

Consider the following discrete-time state-space model of a nonlinear stochastic dynamic system with additive noises

$$\mathbf{x}_{k+1} = \mathbf{f}_k(\mathbf{x}_k, \mathbf{u}_k) + \mathbf{w}_k, \quad k = 0, 1, 2, \dots, T, \quad (1)$$

$$\mathbf{z}_k = \mathbf{h}_k(\mathbf{x}_k) + \mathbf{v}_k, \quad k = 0, 1, 2, \dots, T, \quad (2)$$

where  $\mathbf{x}_k \in \mathbb{R}^{n_x}$ ,  $\mathbf{u}_k \in \mathbb{R}^{n_u}$ , and  $\mathbf{z}_k \in \mathbb{R}^{n_z}$  represent the *unknown* state of the system, *known* input, and measurement at time instant  $k$ , respectively. The state and measurement functions  $\mathbf{f}_k : \mathbb{R}^{n_x \times n_u} \rightarrow \mathbb{R}^{n_x}$  and  $\mathbf{h}_k : \mathbb{R}^{n_x} \rightarrow \mathbb{R}^{n_z}$  are *known* vector transformations. Particular realizations of the state and measurement

<sup>1</sup>The NNMF originally known as non-negative rank factorization or positive matrix factorization has been subject to intensive research for over three decades [16], [17].

noises  $\mathbf{w}_k$  and  $\mathbf{v}_k$  are *unknown*, but their PDFs, i.e., the state noise PDF  $p(\mathbf{w}_k)$  and the measurement noise PDF  $p(\mathbf{v}_k)$ , are *known* as well as the initial state PDF<sup>2</sup>  $p(\mathbf{x}_0)$ . The noises  $\mathbf{w}_k$ ,  $\mathbf{v}_k$ , and the initial condition  $\mathbf{x}_0$  are independent.

### A. Bayesian State Estimation and Recursive Relations

The goal of the state estimation is to find the conditional PDF  $p(\mathbf{x}_k | \mathbf{z}^k)$ ,  $\forall k$  conditioned on all measurements up to the time instant  $k$ , denoted as  $\mathbf{z}^k := [\mathbf{z}_0^T, \mathbf{z}_1^T, \dots, \mathbf{z}_k^T]^T$ , called filtering PDF. The general solution to the state estimation is given by the BRRs for the conditional PDFs<sup>3</sup> computation [22]

$$p(\mathbf{x}_k | \mathbf{z}^k) = \frac{p(\mathbf{x}_k | \mathbf{z}^{k-1})p(\mathbf{z}_k | \mathbf{x}_k)}{p(\mathbf{z}_k | \mathbf{z}^{k-1})}, \quad (3)$$

$$p(\mathbf{x}_{k+1} | \mathbf{z}^k) = \int p(\mathbf{x}_{k+1} | \mathbf{x}_k)p(\mathbf{x}_k | \mathbf{z}^k) d\mathbf{x}_k, \quad (4)$$

where  $p(\mathbf{x}_{k+1} | \mathbf{z}^k)$  is the one-step predictive PDF computed by the Chapman-Kolmogorov equation (CKE) (4) and  $p(\mathbf{x}_k | \mathbf{z}^k)$  is the filtering PDF computed by the Bayes rule (3). The state transient PDF  $p(\mathbf{x}_{k+1} | \mathbf{x}_k) = p_{\mathbf{w}_k}(\mathbf{x}_{k+1} - \mathbf{f}_k(\mathbf{x}_k, \mathbf{u}_k))$  and the measurement PDF  $p(\mathbf{z}_k | \mathbf{x}_k) = p_{\mathbf{v}_k}(\mathbf{z}_k - \mathbf{h}_k(\mathbf{x}_k))$  are obtained from (1) and (2), respectively. The PDF  $p(\mathbf{z}_k | \mathbf{z}^{k-1}) = \int p(\mathbf{x}_k | \mathbf{z}^{k-1})p(\mathbf{z}_k | \mathbf{x}_k) d\mathbf{x}_k$  is the one-step predictive PDF of the measurement. The recursion (3), (4) starts from  $p(\mathbf{x}_0 | \mathbf{z}^{-1}) = p(\mathbf{x}_0)$ .

### B. Grid-Based Density Approximation

The PMF and mPF as grid-based Bayesian filters approximate the conditional PDF  $p(\mathbf{x}_k | \mathbf{z}^m)$ , where  $m = k$  for the filtering PDF and  $m = k - 1$  for the predictive PDF, by a weighted set of grid points

$$p(\mathbf{x}_k | \mathbf{z}^m) \approx \hat{p}(\mathbf{x}_k | \mathbf{z}^m) = \sum_{i=1}^N \omega_{k|m}^{(i)} K(\mathbf{x}_k - \xi_k^{(i)}), \quad (5)$$

where  $K(\mathbf{x}_k - \xi_k^{(i)})$  is a kernel located at grid point  $\xi_k^{(i)} \in \mathbb{R}^{n_x}$  and  $\omega_{k|m}^{(i)}$  is its corresponding weight. The points  $\xi_k^{(i)}$ ,  $i = 1, \dots, N$  form a grid  $\Xi_k = \{\xi_k^{(i)}\}_{i=1}^N$ , which is deterministic and regular for the PMF and random for the mPF.

In the case of the PMF, the kernel is given by a uniform kernel (up to a normalization constant) defined as

$$K(\mathbf{x}_k - \xi_k^{(i)}) = S\{\mathbf{x}_k; \xi_k^{(i)}, \Delta_k\}, \quad (6)$$

with  $S\{\mathbf{x}_k; \xi_k^{(i)}, \Delta_k\}$  being the *selection* function defined as

$$S\{\mathbf{x}_k; \xi_k^{(i)}, \Delta_k\} = \begin{cases} 1, & \text{if } \left| [\mathbf{x}_k]_j - [\xi_k^{(i)}]_j \right| \leq \frac{[\Delta_k]_j}{2}, \\ 0, & \text{otherwise,} \end{cases} \quad (7)$$

<sup>2</sup>If the initial state PDF is unknown, often mean and covariance matrix of the initial state are calculated from the first few measurements and the initial distribution is assumed Gaussian parametrized by the moments [21].

<sup>3</sup>Considering the model (1), (2), the BRRs (3), (4) should also be conditioned on the *available* sequence of the input  $\mathbf{u}_k$ ,  $\forall k$ . However, for the sake of notation simplicity, the input signal is assumed to be implicitly part of the condition and it is not explicitly stated, i.e.,  $p(\mathbf{x}_{k+1} | \mathbf{x}_k) = p(\mathbf{x}_{k+1} | \mathbf{x}_k; \mathbf{u}_k)$ ,  $p(\mathbf{x}_k | \mathbf{z}^k) = p(\mathbf{x}_k | \mathbf{z}^k; \mathbf{u}^{k-1})$ , and  $p(\mathbf{x}_{k+1} | \mathbf{z}^k) = p(\mathbf{x}_{k+1} | \mathbf{z}^k; \mathbf{u}^k)$ .

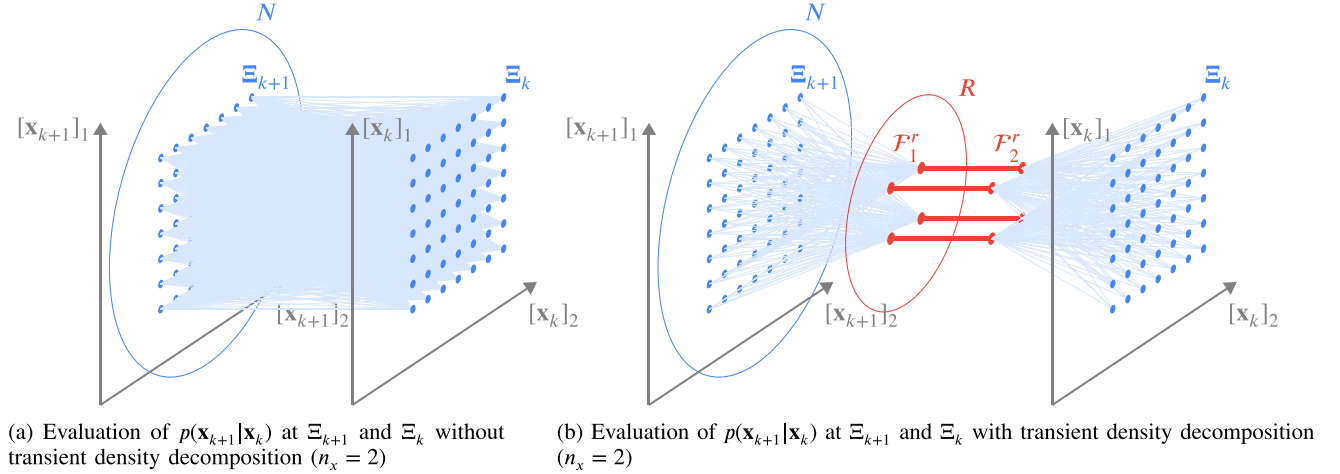


Fig. 1. Illustration of evaluating the predictive PDF without and with transient density decomposition.

where the notation  $[\cdot]_j$  stands for the  $j$ -th element of the involved vector. Thus, the selection is uniform over the  $\Delta_k$ -neighborhood of the grid point  $\xi_k^{(i)}$ . The weight is then given as

$$\omega_{k|m}^{(i)} = P_{k|m}^{(i)} = c_{k|m} \tilde{P}_{k|m}^{(i)}, \quad (8)$$

where  $\tilde{P}_{k|m}^{(i)} = p_{\mathbf{x}_k|\mathbf{z}^m}(\xi_k^{(i)}|\mathbf{z}^m)$  is the conditional PDF  $p(\mathbf{x}_k|\mathbf{z}^m)$  evaluated at the  $i$ -th grid point  $\xi_k^{(i)}$ , and  $c_{k|m} = (\delta_k \sum_{i=1}^N \tilde{P}_{k|m}^{(i)})^{-1}$  is a normalization constant,  $\delta_k = \prod_i [\Delta_k]_i$ .

In the case of the mPF, the kernel is given by a Dirac kernel

$$K(\mathbf{x}_k - \xi_k^{(i)}) = \delta(\mathbf{x}_k - \xi_k^{(i)}), \quad (9)$$

with  $\delta(\cdot)$  being the Dirac delta function. The grid points  $\xi_k^{(i)}$  are called particles and the weights  $\omega_{k|m}^{(i)}$  are normalized to one.

### C. Chapman-Kolmogorov Equation Computation

Computing the predictive weights  $\{\omega_{k+1|k}^{(j)}\}_{j=1}^N$  for grid-based predictive PDF approximation  $\hat{p}(\mathbf{x}_{k+1}|\mathbf{z}^k)$  in the PMF (see e.g., [19]) and the mPF (see e.g., [20]) requires evaluation of the predictive PDF given by the CKE (4) at the grid points  $\mathbf{x}_{k+1} = \xi_{k+1}^{(j)}$ ,  $j = 1, \dots, N$  as

$$p(\xi_{k+1}^{(j)}|\mathbf{z}^k) = \int p(\xi_{k+1}^{(j)}|\mathbf{x}_k) \sum_{i=1}^N \omega_{k|k}^{(i)} K(\mathbf{x}_k - \xi_k^{(i)}) d\mathbf{x}_k, \quad (10)$$

where the filtering PDF  $p(\mathbf{x}_k|\mathbf{z}^k)$  is approximated as (5). Thus, the state transient PDF  $p(\mathbf{x}_{k+1}|\mathbf{x}_k)$  is evaluated for all combinations of the grid points  $\Xi_{k+1}$  and  $\Xi_k$  (see Fig. 1(a)). When using a large number of grid points, such evaluation constitutes a bottleneck for both PMF and mPF standard implementations. This paper proposes a transient PDF decomposition to reduce the computational costs of convolution calculations.

### III. TRANSIENT DENSITY DECOMPOSITION

Assume that the state transient PDF can be decomposed as

$$p(\mathbf{x}_{k+1}|\mathbf{x}_k) \approx \sum_{r=1}^R \mathcal{F}_1^r(\mathbf{x}_{k+1}) \mathcal{F}_2^r(\mathbf{x}_k), \quad (11)$$

where  $\mathcal{F}_1^r(\cdot)$ ,  $\mathcal{F}_2^r(\cdot)$ ,  $r = 1, \dots, R$  are suitable (non-negative) functions, known in advance, and  $R$  is the order of the approximation called *rank*.<sup>4</sup> The decomposition (11) is “efficient” if  $R$  is small and the approximation error is small as well. There is always a trade-off between the complexity of the approximation ( $R$ ) and the error. Later in the paper, we show that the trade-off is “good” in the case of the Gaussian transients and in the case of non-Gaussian distribution with heavier tails, which can be encountered in the literature [24].

Given (11), the CKE (4) can be written as

$$p(\mathbf{x}_{k+1}|\mathbf{z}^k) \approx \sum_{r=1}^R \mathcal{F}_1^r(\mathbf{x}_{k+1}) \int \mathcal{F}_2^r(\mathbf{x}_k) p(\mathbf{x}_k|\mathbf{z}^k) d\mathbf{x}_k. \quad (12)$$

The simplification of (12) w.r.t. (10) is that  $R$  integrals in (4) can be computed at the grid points  $\Xi_k$  only, without the need of considering the combination of all grid points  $\Xi_{k+1}$  for  $\mathbf{x}_{k+1}$  and all grid points  $\Xi_k$  for  $\mathbf{x}_k$ .

For the point-mass approximation (6) of  $p(\mathbf{x}_k|\mathbf{z}^k)$  the integral in (12) is

$$\int \mathcal{F}_2^r(\mathbf{x}_k) p(\mathbf{x}_k|\mathbf{z}^k) d\mathbf{x}_k \approx \sum_{i=1}^N \mathcal{F}_2^r(\xi_k^{(i)}) P_{k|k}^{(i)} \delta_k =: \mathcal{I}_k^r. \quad (13)$$

The values of the predictive PDF (12) are then given as

$$\tilde{P}_{k+1|k}^{(j)} = \sum_{r=1}^R \mathcal{F}_1^r(\xi_{k+1}^{(j)}) \mathcal{I}_k^r. \quad (14)$$

Obtaining values  $\tilde{P}_{k+1|k}^{(j)}$  of  $\hat{p}(\mathbf{x}_{k+1}|\mathbf{z}^k)$  for all grid points  $\Xi_{k+1}$  then requires:

- 1) evaluating  $R$  functions  $\mathcal{F}_2^r$  at  $\{\xi_k^{(i)}\}_{i=1}^N$ ,
- 2) combining their values with the weights in (13) to obtain  $\mathcal{I}_k^r$ ,
- 3) evaluating  $R$  functions  $\mathcal{F}_1^r$  at  $\{\xi_{k+1}^{(j)}\}_{j=1}^N$ ,
- 4) obtaining the approximate transient PDF values through (14).

<sup>4</sup>The relation (11) can be seen as a special case of the functional tensor decomposition [23] where the functions  $\mathcal{F}_1^r$  and  $\mathcal{F}_2^r$  are not decomposed further to functions of single elements of  $\mathbf{x}_{k+1}$  and  $\mathbf{x}_k$ .

The whole process can be illustrated for the two-dimensional state with  $N = 7^2 = 49$  grid points  $\{\xi_k^i\}_{i=1}^N$  and rank  $R = 4$  by Fig. 1.

For the particle approximation (9) of  $p(\mathbf{x}_k|\mathbf{z}^k)$ , the integral in (12) is

$$\int \mathcal{F}_2^r(\mathbf{x}_k)p(\mathbf{x}_k|\mathbf{z}^k)d\mathbf{x}_k \approx \sum_{i=1}^N \mathcal{F}_2^r(\xi_k^{(i)})\omega_{k|k}^{(i)}. \quad (15)$$

Calculation of the predictive weights  $\omega_{k+1}^{(i)}$  then requires the same procedure described above. More details about using the decomposition in the mPF can be found in [20].

Note that in some cases, the functions  $\mathcal{F}_1^r(\cdot)$  and  $\mathcal{F}_2^r(\cdot)$ , have the same functional form for  $r = 1, \dots, R$ , i.e.  $\mathcal{F}_1^1 = \mathcal{F}_1^2 = \dots = \mathcal{F}_1^R$  and  $\mathcal{F}_2^1 = \mathcal{F}_2^2 = \dots = \mathcal{F}_2^R$ , and differ only in the value of a vector/scalar parameter  $\theta$  so that

$$\mathcal{F}_1^r(\mathbf{x}_k) = \mathcal{F}_1(\mathbf{x}_k; \theta_1^r), \quad (16)$$

$$\mathcal{F}_2^r(\mathbf{x}_{k+1}) = \mathcal{F}_2(\mathbf{x}_{k+1}; \theta_2^r). \quad (17)$$

Such a case is demonstrated in Section III-C, where the functions  $\mathcal{F}_1^r$  and  $\mathcal{F}_2^r$  both have Gaussian bell-curve shape parametrized by its location, width, and height.

#### A. Finding the Decomposition

The decomposition in (11) can be found by the following procedure: First, fixed grids of points  $\Psi_{k+1}$  and  $\Psi_k$  representing  $\mathbf{x}_{k+1}$  and  $\mathbf{x}_k$ , respectively and covering regions of interest  $\Omega_{k+1} \subset \mathbb{R}^{n_x}$  and  $\Omega_k \subset \mathbb{R}^{n_x}$ , respectively, are constructed and the transition PDF is evaluated at the grid points (Remind that  $p_{\mathbf{x}_{k+1}|\mathbf{x}_k} : \mathbb{R}^{n_x} \times \mathbb{R}^{n_x} \rightarrow \mathbb{R}$ ). Then, the resulting tensor is decomposed using the well-known task of NNMF or non-negative tensor factorization. Note that this decomposition used optimization w.r.t. L2 norm.

Next, a suitable rank  $R$  of the decomposition is determined. It should be selected to achieve a compromise between the computational complexity of the approximation and the approximation error. As a rule of thumb, we can determine a suitable rank as the number of significant singular values of the matrix as will be shown later.

Once the decomposition (11) is obtained for the fixed grid, it can be interpolated to give a similar decomposition in the continuous domain  $\Omega_{k+1} \times \Omega_k$ , which defines the closed approximation region. The interpolation can be numerical, e.g., spline, or functional. In the examples, we use interpolation functions  $\mathcal{F}_1^r(\cdot)$  and  $\mathcal{F}_2^r(\cdot)$  with parameters  $\theta_1^r$  and  $\theta_2^r$  that are found off-line by an optimization procedure. The procedure minimizes a norm of the difference of the original transient PDF and the functional approximation (11) with (16) over the approximation region. The L1 norm seems natural when dealing with PDFs, but its computation may be computationally prohibitive for higher state dimensions. In such cases, we use the L2 norm instead. The L2 norm is highly large-error dominant and thus more prone to outliers than L1 norm. The L1 norm, is more robust towards outliers than L2 norm, as it does not overstate errors. The error expressed using L1 norm aligns with the original degree of the

variable, which is the PDF in this case. Throughout this paper, we use the Nelder-Mead algorithm [25] for the minimization.

#### B. Simplification for Additive State Noise

The functions  $\mathcal{F}_1^r(\cdot)$  and  $\mathcal{F}_2^r(\cdot)$  (or their parameters  $\theta_1^r$  and  $\theta_2^r$ ) may change with position of regions of interest. For the additive state noise (1), a simplification of the decomposition calculation can be achieved. In such a case, the transient PDF  $p(\mathbf{x}_{k+1}|\mathbf{x}_k) = p_{\mathbf{w}_k}(\mathbf{x}_{k+1} - \mathbf{f}_k(\mathbf{x}_k, \mathbf{u}_k))$  can be interpreted as a function of  $\mathbf{x}_{k+1}$  and  $\mathbf{f}_k$ , where  $\mathbf{f}_k = \mathbf{f}_k(\mathbf{x}_k, \mathbf{u}_k)$  denotes the value of the function  $\mathbf{f}_k$  for convenience. The value of the transient PDF thus depends only on the difference of  $\mathbf{x}_{k+1}$  and  $\mathbf{f}_k$ , i.e.,  $p(\mathbf{x}_{k+1}|\mathbf{x}_k) = p_{\mathbf{w}_k}(\mathbf{x}_{k+1} - \mathbf{f}_k)$ . Subsequently, the decomposition (11) in the form

$$p_{\mathbf{w}_k}(\mathbf{x}_{k+1} - \mathbf{f}_k) \approx \sum_{r=1}^R \mathcal{F}_1^r(\mathbf{x}_{k+1})\mathcal{F}_2^r(\mathbf{f}_k) \quad (18)$$

needs to be computed on the basis of a time-invariant grid  $\Psi \times \Psi$  covering a fixed region of interest  $\Omega \times \Omega \in \mathbb{R}^{n_x} \times \mathbb{R}^{n_x}$  for  $[\mathbf{x}_{k+1}^T, \mathbf{f}_k^T]^T$ . The region of interest  $\Omega \times \Omega$  is fixed as only the difference  $\mathbf{x}_{k+1} - \mathbf{f}_k$  matters.

If the value (18) needs to be evaluated for grids corresponding to  $\mathbf{x}_{k+1}$  and  $\mathbf{f}_k$  that are far from the approximation region, they can be both shifted by some  $\zeta$  towards the center of the approximation region as  $p_{\mathbf{w}_k}(\mathbf{x}_{k+1} - \mathbf{f}_k) = p_{\mathbf{w}_k}((\mathbf{x}_{k+1} - \zeta) - (\mathbf{f}_k - \zeta))$ . This is highly beneficial for the reduction of costs of the decomposition computation, which can be calculated prior to the estimation itself and does not affect the PMF or mPF costs.

Additionally, if the function  $p_{\mathbf{w}_k}(\mathbf{x}_{k+1} - \mathbf{f}_k)$  is symmetric in the sense that it is invariant with respect to a permutation of its arguments  $\mathbf{x}_{k+1}$  and  $\mathbf{f}_k$ , we may assume that the decomposition (18) is symmetric as well, i.e.,  $\mathcal{F}_1^r = \mathcal{F}_2^r$  (or  $\theta_1^r = \theta_2^r$ ) for  $r = 1, \dots, R$ . Note that if the process noise does not act additively in the state dynamics (1), the transient PDF could be complicated and time-varying, which may require the calculation of the decomposition at each time instant. This may have an adverse effect on the computational costs of the PMF.

#### C. Univariate Gaussian Transient PDF

This section demonstrates the decomposition for the univariate Gaussian transient PDF, which is symmetric. For convenience, consider process noise variance  $\text{var}[w_k] = Q = 1$

$$p(x_{k+1}|x_k) = p_{w_k}(x_{k+1} - f_k) = \frac{1}{\sqrt{2\pi}} e^{-\frac{1}{2}(x_{k+1}-f_k)^2}. \quad (19)$$

Consider a region  $\Omega \subset \mathbb{R}^2$  for  $[x_{k+1}, f_k]^T$  given by the ranges  $x_{k+1} \in [-L, L]$ ,  $f_k \in [-L, L]$ ,  $L = 10$ , with granularity  $1/10$  to obtain a  $D \times D$  grid  $\Psi$ ,  $D = 201$ . Then, the state transient PDF (19) is evaluated at its points, which results in the matrix  $\mathbf{M} \in \mathbb{R}^{D \times D}$ . This matrix is subject to an NNMF  $\mathbf{M} = \mathbf{W}\mathbf{H}$  or, better, a symmetric NNMF  $\mathbf{M} = \mathbf{W}\mathbf{W}^T$ , where  $\mathbf{W} \in \mathbb{R}^{D \times R}$  and  $\mathbf{H} \in \mathbb{R}^{R \times D}$  are matrices with non-negative elements and  $R$  is the rank. Here, due to the symmetricity, the algorithm of [18] is utilized.

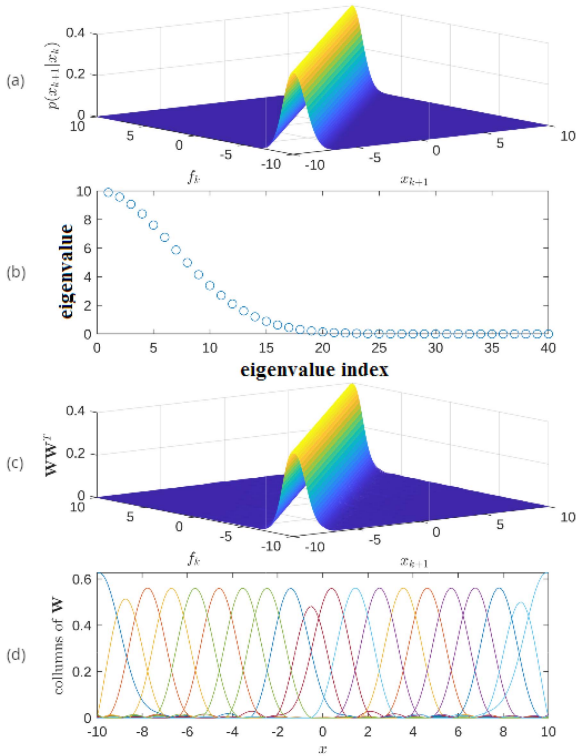


Fig. 2. (a) Original transient PDF, (b) leading eigenvalues of  $\mathbf{M}$ , (c) an approximate transient PDF for  $R = 20$ , and (d) columns of  $\mathbf{W}$  for  $R = 20$  obtained by NNMF.

A suitable rank<sup>5</sup>  $R$  of the approximation  $\mathbf{W}\mathbf{W}^T$  can be deduced from the number of leading eigenvalues of  $\mathbf{M}$ .

For illustration, the matrix  $\mathbf{M}$  (i.e., the transient PDF (19) evaluated at  $\Psi$ ) and 40 of its largest eigenvalues are plotted in Fig. 2. The eigenvalues suggest that a good approximation could be obtained for ranks  $R \geq 20$ . An approximate transient PDF for  $R = 20$  and curves depicting 20 columns of  $\mathbf{W}$  are shown in Fig. 2. The values in columns of  $\mathbf{W}$  representing values of  $\mathcal{F}_1^r = \mathcal{F}_2^r$ ,  $r = 1, \dots, R$  at grid  $\Psi$  have the Gaussian bell-curve shapes, roughly uniformly distributed<sup>6</sup> within the interval  $[-L, L]$ . Hence, the columns of  $\mathbf{W}$  will be modeled by the functions  $\mathcal{F}_1^r(\cdot) = \mathcal{F}_2^r(\cdot) = \mathcal{F}(\cdot; \theta^r)$  as

$$\mathcal{F}(x; \theta^r) = \beta \cdot e^{-\frac{1}{2}(x-\mu^r)^2/\sigma^2} \quad (20)$$

parameterized by the peak position  $\mu^r$ , width  $\sigma$ , and height  $\beta$ , i.e.,  $\theta^r = [\mu^r, \sigma, \beta]$ . Notice that due to the shapes of the curves for each column of  $\mathbf{W}$ , the parameters  $\beta$  and  $\sigma$  are the same for  $r = 1, \dots, R$ . Given the range  $2L$ , rank  $R$ , and regularity of the peak distribution, the distance of the adjacent peaks will be fixed to  $d = \mu^r - \mu^{r-1}$ ,  $r = 2, \dots, R$ , where  $d = 2L/(R-1)$  is the distance between the adjacent peaks. The other two parameters

<sup>5</sup>Note that the rank of a decomposition of a matrix is a lower bound of the rank of the *non-negative* decomposition of the matrix, in general.

<sup>6</sup>A minor difference can be spotted close to  $x = 0$ , and close to the region boundaries. The boundaries are rather unimportant in this problem; they are related to the ranges of  $x_{k+1}$  and  $f_k$ , which can be easily adjusted to make sure that the values  $x_{k+1}$  and  $f_k$  will remain in this range.

TABLE I  
PEAK DISTANCES, RANK, WIDTHS, HEIGHTS, AND THE MEAN ABSOLUTE ERROR OF THE TRUE AND APPROXIMATE TRANSIENT PDF DECOMPOSITION OBTAINED BY NUMERICAL OPTIMIZATION FOR UNIVARIATE GAUSSIAN DISTRIBUTION

$d$	$R$	$\sigma$	$\beta$	$E$ (L1 norm)
0.5	41	0.7071	0.3989	$2.8773 \times 10^{-6}$
0.6	34	0.7071	0.4370	$2.1009 \times 10^{-6}$
0.7	29	0.7071	0.4720	$5.5075 \times 10^{-6}$
0.8	26	0.7071	0.5046	$3.0482 \times 10^{-5}$
1.0	20	0.7077	0.5638	$4.8372 \times 10^{-4}$
1.33	16	0.7306	0.6271	$3.7326 \times 10^{-3}$
2.0	10	0.8494	0.6432	$1.3456 \times 10^{-2}$

$\sigma$  and  $\beta$  will be obtained by the numerical optimization (the Nelder-Mead algorithm [25]) to minimize the average absolute error (denoted by  $E$ ) between the true transient PDF and its approximation (19). The results of the optimization are listed in Table I. From the table, it follows that the error  $E$  decreases with increasing rank. However, for  $R > 30$  the shape of the curves deviates significantly from the Gaussian bell-curve shape, and the error does not decrease anymore. The result (20) can be generalized for arbitrary variance  $Q$  and arbitrary range  $L$ , as it is shown in section III-H. A simple scale transformation converts the case with the general  $Q$  in the case of  $Q = 1$ . The transformation implies that the appropriate rank  $R'$ , distance of the adjacent peak positions  $d'$ , and the height  $\beta'$  and width  $\sigma'$  of the terms in (20) would be

$$R' = \left\lfloor \frac{2L}{\sqrt{Q}} \right\rfloor, \quad d' = d\sqrt{Q}, \quad \beta' = \frac{\beta}{\sqrt[4]{Q}}, \quad \sigma' = \sigma\sqrt{Q}. \quad (21)$$

We note that the approximation of the transient PDF is accurate in the interior of the lattice of the peaks. At each point, only a few peaks located closest to the point contribute to the PDF approximation. As the peaks outside the boundary are not present, the approximation may be less accurate close to the boundary of the lattice. Outside the lattice, the approximation is poor and converges quickly to zero for increasing distance from the lattice. This is a very general pattern that applies not only to Gaussian distribution but to other distributions as well.

#### D. Student T-Distributed Transient PDF

In this section, we repeat the previous procedure for the Student t-distributed transient PDF that was studied, e.g., in [24]. This PDF has heavier tails than the Gaussian distribution. We have chosen the distribution with three degrees of freedom<sup>7</sup> (DoF), which has the density

$$p(x_{k+1}|x_k) = p_{w_k}(x_{k+1} - f_k) = \frac{2}{\pi\sqrt{3}[1 + (x_{k+1} - f_k)^2/3]^2}.$$

The Student t-distributed transient PDF, leading eigenvalues of  $\mathbf{M}$ , approximate transient PDF, and columns of  $\mathbf{W}$  are shown in Fig. 3. We can see that roughly the same accuracy as for Gaussian transient is attained for a slightly higher rank, between

<sup>7</sup>This DoF is the smallest value, for which the mean and variance are defined. For large DoF, the Student t-distribution approaches the Gaussian distribution.

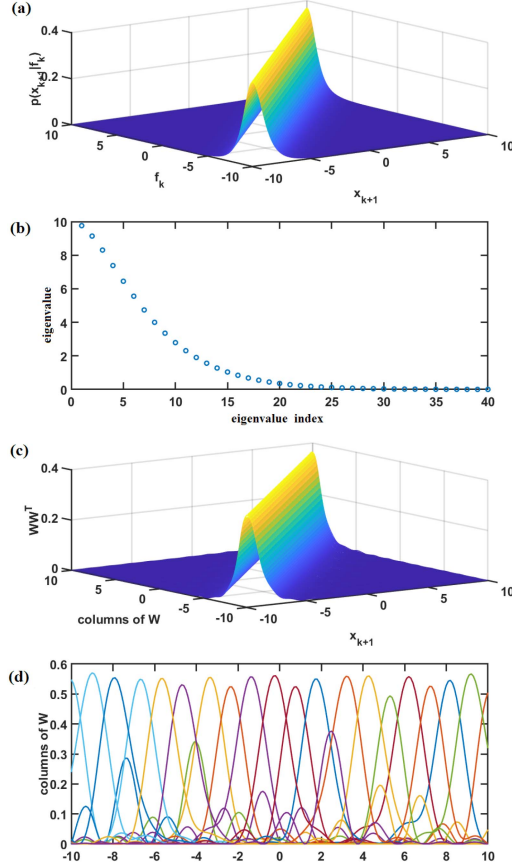


Fig. 3. (a) Student t-distributed transient PDF with DoF 3, (b) leading eigenvalues of  $\mathbf{M}$ , (c) an approximate transient PDF for  $R = 25$ , and (d) columns of  $\mathbf{W}$  for  $R = 25$  obtained by NNMF.

25 and 30. Columns of the matrix  $\mathbf{W}$  have a form of peaks, now with certain sidelobes.

The peaks have a shape similar to that of the original transient PDF. Therefore, we shall model them as

$$\mathcal{F}^r(x) = \frac{\beta}{(1 + (x - \mu^r)^2/\sigma^2)^\alpha}. \quad (22)$$

It means that each peak is parametrized by the height  $\beta$ , the width  $\sigma$ , location  $\mu^r$ , and the exponent  $\alpha$ . The peak locations are regularly distributed with distance  $d$  between the adjacent peaks. The optimum values  $\sigma$ ,  $\alpha$  and  $\beta$  for various values of  $d$  are listed in Table II. The mean error  $E$  is computed over interior of  $\Omega$ , in the region given by  $x_{k+1} \in [-9, 9]$  and  $f_k \in [-9, 9]$ .

### E. Cauchy-Distributed Transient PDF

In this section, we repeat the previous procedure for the Cauchy-distributed transient PDF that was mentioned, e.g., in [26]. This PDF still has heavier tails than the Student-t distribution. It has the density

$$p(x_{k+1}|x_k) = p_{w_k}(x_{k+1} - f_k) = \frac{1}{\pi} \frac{1}{1 + (x_{k+1} - f_k)^2}.$$

The peaks in the decomposition will be modeled as those in (22), which seems flexible enough. The difference is only in

TABLE II  
PEAK DISTANCES, RANK, WIDTHS, ALPHAS, HEIGHTS, AND THE MEAN ABSOLUTE ERROR OF THE TRUE AND APPROXIMATE TRANSIENT PDF DECOMPOSITION OBTAINED BY NUMERICAL OPTIMIZATION FOR UNIVARIATE STUDENT T-DISTRIBUTION

$d$	$R$	$\sigma$	$\alpha$	$\beta$	$E$ (L1 norm)
0.5	41	0.9180	1.6869	0.4279	$1.6559 \times 10^{-4}$
0.6	34	0.9234	1.6944	0.4675	$2.1057 \times 10^{-4}$
0.7	29	0.9314	1.7057	0.5031	$3.7186 \times 10^{-4}$
0.8	26	0.9448	1.7235	0.5341	$7.0448 \times 10^{-4}$
1.0	20	0.9861	1.7725	0.5827	$1.9420 \times 10^{-3}$
1.33	16	1.1627	1.9948	0.6109	$4.9733 \times 10^{-3}$
2.0	10	3.8176	9.6271	0.5986	$2.2656 \times 10^{-2}$

TABLE III  
PEAK DISTANCES, RANK, WIDTHS, ALPHAS, HEIGHTS, AND THE MEAN ABSOLUTE ERROR OF THE TRUE AND APPROXIMATE TRANSIENT PDF DECOMPOSITION OBTAINED BY NUMERICAL OPTIMIZATION FOR UNIVARIATE CAUCHY DISTRIBUTION

$d$	$R$	$\sigma$	$\alpha$	$\beta$	$E$ (L1 norm)
0.5	41	0.3616	0.7866	0.2370	$2.2151 \times 10^{-3}$
0.6	34	0.3889	0.8293	0.2737	$2.8238 \times 10^{-3}$
0.7	29	0.4833	0.9616	0.2814	$3.1382 \times 10^{-3}$
0.8	26	0.5233	1.0007	0.2976	$3.4546 \times 10^{-3}$
1.0	20	0.6097	1.0705	0.3137	$4.3390 \times 10^{-3}$
1.33	16	0.7283	1.1368	0.3216	$6.1191 \times 10^{-3}$
2.0	10	0.9228	1.2111	0.3185	$1.023 \times 10^{-2}$

error and the optimum parameters. The results are summarized in Table III. The mean error  $E$  is computed over interior of  $\Omega$ , in the region given by  $x_{k+1} \in [-9, 9]$  and  $f_k \in [-9, 9]$ . We note that the fitting error is, indeed, greater than in the case of Student or Gaussian distributions.

### F. Multivariate Gaussian Transient PDF for $n_x = 2$

In this section, the assumption of a scalar state is dropped and  $n_x = 2$  is assumed. Then, for a zero-mean Gaussian noise  $\mathbf{w}_k$  with the covariance matrix  $\text{cov}[\mathbf{w}_k] = \mathbf{Q}$ , the transient PDF is

$$\begin{aligned} p(\mathbf{x}_{k+1}|\mathbf{x}_k) &= p_{\mathbf{w}_k}(\mathbf{x}_{k+1} - \mathbf{f}_k) \\ &= \frac{1}{\sqrt{(2\pi)^{n_x} |\mathbf{Q}|}} e^{-\frac{1}{2}(\mathbf{x}_{k+1} - \mathbf{f}_k)^T \mathbf{Q}^{-1}(\mathbf{x}_{k+1} - \mathbf{f}_k)}. \end{aligned}$$

Assume first, for simplicity, that  $\mathbf{Q}$  is the identity matrix. Then,

$$\begin{aligned} p_{\mathbf{w}_k}(\mathbf{x}_{k+1} - \mathbf{f}_k) &= \frac{1}{2\pi} e^{-\frac{1}{2}(\mathbf{x}_{k+1} - \mathbf{f}_k)^T (\mathbf{x}_{k+1} - \mathbf{f}_k)} \\ &= \frac{1}{2\pi} e^{-\frac{1}{2}[(\mathbf{x}_{k+1} - \mathbf{f}_k)_1]^2 + [(\mathbf{x}_{k+1} - \mathbf{f}_k)_2]^2} \\ &= p((\mathbf{x}_{k+1})_2 | [(\mathbf{f}_k)_2]) p((\mathbf{x}_{k+1})_1 | [(\mathbf{f}_k)_1]). \end{aligned} \quad (23)$$

In Section III-C, we have shown that each term  $p((\mathbf{x}_{k+1})_i | [(\mathbf{f}_k)_i])$ ,  $i = 1, 2$  can be decomposed as a sum of  $R$  terms  $\mathcal{F}_1^r \mathcal{F}_2^r$ .

The direct product of two one-dimensional decompositions each having  $R_1$  terms would require  $R = (R_1)^2$  terms  $\mathcal{F}_1^{r_1} \mathcal{F}_2^{r_2} \mathcal{F}_1^{r_1} \mathcal{F}_2^{r_2}$ . It means that the effective rank of such decomposition is  $(R_1)^2$  through peaks arranged in a rectangular lattice, see Fig. 4, left diagram. The grid can be written symbolically as  $[-L : d : L] \otimes [-L : d : L]$ . This approach was proposed in [19].

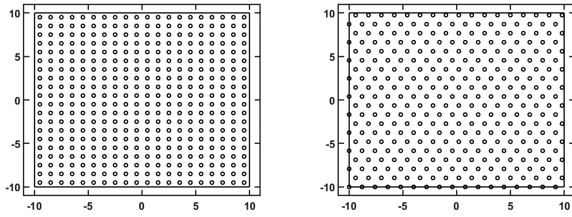


Fig. 4. Rectangular and triangular lattices of peaks.

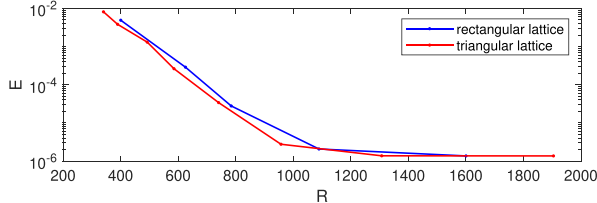


Fig. 5. Mean absolute error versus the rank.

The rectangular lattice is not, however, optimal in the sense of packing circles representing the functions  $\mathcal{F}(\mathbf{x}, \theta^r)$  on a 2D surface.<sup>8</sup> The highest-density lattice packing of circles can be obtained for a triangular lattice, where the vertices are the centers of the densest possible circle packing [27]. The triangular lattice covers the area of interest more efficiently by increasing rank while preserving a minimum distance between adjacent vertices. It can be written as a union of two rectangular grids,  $([-L : d : L] \otimes [-L : d_1 : L]) \cup ([-L + d/2 : d : L] \otimes [-L + d_1/2 : d_1 : L])$ , where  $d_1 = d\sqrt{3}$ , see Fig. 4, right diagram.

We show that with the same number of peaks the triangular lattice of peaks reduces the error of the approximation for the rectangular lattice or, vice versa, the same approximation error for both lattices can be obtained with a lower number of peaks for the triangular lattice, see Fig. 5.

In both cases, the transient PDF in (23) is approximated as

$$p(\mathbf{x}_{k+1}|\mathbf{x}_k) \approx \sum_{r=1}^R \mathcal{F}(\mathbf{x}_{k+1}; \theta^r) \mathcal{F}(\mathbf{f}_k; \theta^r) \quad (24)$$

where  $R$  is the number of peaks and

$$\mathcal{F}(\mathbf{x}; \theta^r) = \beta^{n_x} \cdot e^{-\frac{\|\mathbf{x} - \boldsymbol{\mu}^r\|^2}{2\sigma^2}} \quad (25)$$

$$= \beta^2 \cdot e^{-\frac{1}{2\sigma^2} [(\mathbf{x}_1 - [\boldsymbol{\mu}^r]_1)^2 + (\mathbf{x}_2 - [\boldsymbol{\mu}^r]_2)^2]} \quad (26)$$

with  $\theta^r = [(\boldsymbol{\mu}^r)^T, \sigma, \beta]$ . The approximation in (24) can be very accurate if both  $\mathbf{x}_{k+1}$  and  $\mathbf{f}_k$  lie in the interior of the lattice. Close to its boundary, the error is somewhat larger. The parameters  $\sigma$  and  $\beta$  are found by optimizing the average absolute error of the approximation in the interior, specified by the range  $[-9, 9] \times [-9, 9]$ . The  $d$  represents the distance of the adjacent peaks. The result of the optimization is presented in Table IV. We can see that for  $d \in [0.5, 0.8]$  the optimum value of  $\sigma$  is approximately  $0.7071 \approx \sqrt{0.5}$ . It is the same value that was achieved in the

<sup>8</sup>The functions  $\mathcal{F}$  are even-symmetric, i.e., for example for  $n_x = 2$ , the contours of the functions are circles. Circle packing then concerns the most efficient way of covering a region in the plane by such circles

TABLE IV  
PEAK DISTANCES, RANK, WIDTHS, HEIGHTS, AND THE MEAN ABSOLUTE ERROR OF THE TRUE (GAUSSIAN) AND APPROXIMATE TRANSIENT PDF DECOMPOSITION FOR  $n_x = 2$ , OBTAINED BY NUMERICAL OPTIMIZATION

	$d$	$R$	$\sigma$	$\beta$	$E$ (L1 norm)
triangular lattice	0.5	1904	0.7071	0.3847	$1.37 \times 10^{-6}$
	0.6	1307	0.7071	0.4217	$1.38 \times 10^{-6}$
	0.7	957	0.7071	0.4554	$2.77 \times 10^{-6}$
	0.8	740	0.7071	0.4869	$3.42 \times 10^{-5}$
	0.9	585	0.7072	0.5162	$2.64 \times 10^{-4}$
	1.0	492	0.7072	0.5442	$1.31 \times 10^{-3}$
	1.1	389	0.7081	0.5702	$3.84 \times 10^{-3}$
rectangular lattice	1.2	340	0.7118	0.5932	$8.15 \times 10^{-3}$
	0.5	1600	0.7071	0.3989	$1.37 \times 10^{-6}$
	0.6	1089	0.7071	0.4370	$2.08 \times 10^{-6}$
	0.7	784	0.7071	0.4717	$2.79 \times 10^{-5}$
	0.8	625	0.7071	0.5046	$2.89 \times 10^{-4}$
	1.0	400	0.7088	0.5635	$4.91 \times 10^{-3}$

one-dimensional optimization in Table I. Note that the case of general  $\mathbf{Q}$  will be treated later in Section III-H.

### G. Multivariate Gaussian Transient PDF for $n_x > 2$

In dimensions greater than 2, the decomposition of the transient PDF proceeds similarly to  $n_x = 2$ . Again, it is possible to consider a rectangular lattice of peaks, or a triangular one. In 3D, the peaks will be arranged as vertices of regular tetrahedrons. The key parameter is the distance of the adjacent peaks,  $d$ . In the rectangular grid in 3D, each peak has 6 adjacent peaks of the same distance. In the triangular grid in 3D, there are 12 adjacent peaks of the same distance. Six of them lie in one plane, three above the plane and the other three below the plane. In 3D, the triangular lattice can be built as a union of four rectangular lattices. In 4D, it is composed of eight rectangular lattices. The lattices can be constructed recursively, using shifts of lattices of lower dimensions. Let  $\mathcal{L}_n = \mathcal{L}_n(L, d)$  denote the triangular lattice in dimension  $n$ , i.e., a collection of  $n$ -dimensional vectors,  $\mathcal{L}_n + [x_1, \dots, x_n]$  be a shift of the grid. Then,

$$\mathcal{L}_1(L, d) = [-L : d : L],$$

$$\begin{aligned} \mathcal{L}_2(L, d) &= \mathcal{L}_1(L, d) \otimes [-L : d_1 : L] \\ &\cup (\mathcal{L}_1 + d/2) \otimes [-L + d_1/2 : d_1 : L], \end{aligned}$$

$$\begin{aligned} \mathcal{L}_3(L, d) &= \mathcal{L}_2(L, d) \otimes [-L : d_2 : L] \\ &\cup (\mathcal{L}_2 + [d/2, d_1/6]) \otimes [-L + d_2/2 : d_2 : L], \end{aligned}$$

$$\begin{aligned} \mathcal{L}_4(L, d) &= \mathcal{L}_3(L, d) \otimes [-L : d_3 : L] \\ &\cup (\mathcal{L}_3 + [d/2, d_1/6, d_2/8]) \otimes [-L + d_3/2 : d_3 : L], \end{aligned}$$

where  $d_1 = d\sqrt{3}$ ,  $d_2 = d\sqrt{8/3}$ , and  $d_3 = d\sqrt{2}$ . Similarly to the 2D case, the triangular lattice provides, with the same number of peaks, smaller fitting errors than the rectangular one.

In dimensions 3 and higher, it is costly to compute the fitting error through the L1 norm, as we did before, and consequently to compute the optimum parameters of the peaks. If the system state has dimension 3, the transient function lives in dimension 6, and if we want to compute the approximation error on the grid with

TABLE V  
PEAK DISTANCES, PEAK NUMBER (RANK COMPUTED FOR THE AREA OF INTEREST  $7 \times 7 \times 7$ ), WIDTHS, HEIGHTS, AND L2 ERROR OF THE TRUE (GAUSSIAN) AND APPROXIMATE TRANSIENT PDF DECOMPOSITION FOR  $n_x = 3$  COMPUTED IN THE DOMAIN  $[-1, 1]^3 \times [-\infty, \infty]^3$

	$d$	$R$	$\sigma$	$\beta$	$E$ (L2 norm)
triangular lattice	0.5	32413	0.7071	0.3766	$1.54 \times 10^{-11}$
	0.6	18055	0.7071	0.4125	$1.55 \times 10^{-11}$
	0.7	12027	0.7071	0.4455	$1.65 \times 10^{-11}$
	0.8	8118	0.7071	0.4763	$3.71 \times 10^{-10}$
	0.9	5600	0.7071	0.5052	$2.93 \times 10^{-8}$
	1.0	4331	0.7071	0.5329	$7.29 \times 10^{-7}$
	1.1	3016	0.7074	0.5584	$8.24 \times 10^{-6}$
1.2	2424	0.7086	0.5824	$5.34 \times 10^{-5}$	
rectangular lattice	0.5	21952	0.7071	0.3989	$1.59 \times 10^{-11}$
	0.6	12167	0.7071	0.4370	$1.67 \times 10^{-11}$
	0.7	8000	0.7071	0.4720	$1.95 \times 10^{-9}$
	0.8	4913	0.7071	0.5046	$2.16 \times 10^{-7}$
	0.9	3375	0.7073	0.5351	$5.49 \times 10^{-6}$
	1.0	2744	0.7085	0.5633	$5.46 \times 10^{-5}$

TABLE VI  
PEAK DISTANCES, PEAK NUMBER (RANK COMPUTED FOR THE AREA OF INTEREST  $7 \times 7 \times 7 \times 7$ ), WIDTHS, HEIGHTS, AND L2 ERROR OF THE TRUE (GAUSSIAN) AND APPROXIMATE TRANSIENT PDF DECOMPOSITION FOR  $n_x = 4$  COMPUTED IN THE DOMAIN  $[-1, 1]^4 \times [-\infty, \infty]^4$

	$d$	$R$	$\sigma$	$\beta$	$E$ (L2 norm)
triangular lattice	0.7	338829	0.7071	0.4328	$7.17 \times 10^{-12}$
	0.8	190874	0.7071	0.4628	$5.43 \times 10^{-11}$
	0.9	123552	0.7071	0.4908	$3.68 \times 10^{-9}$
	1.0	82550	0.7071	0.5174	$1.06 \times 10^{-7}$
	1.1	55224	0.7072	0.5466	$1.20 \times 10^{-6}$
	1.2	40824	0.7075	0.5666	$9.53 \times 10^{-6}$
rectangular lattice	0.7	160000	0.7071	0.4721	$1.46 \times 10^{-9}$
	0.8	83521	0.7071	0.5047	$1.63 \times 10^{-7}$
	0.9	50625	0.7073	0.5351	$4.13 \times 10^{-6}$
	1.0	38416	0.7085	0.5633	$4.11 \times 10^{-5}$

40 points along each axis, it is  $40^6$  points. The computation of the error of each of these points involves hundreds or thousands of peaks, so it is computationally intensive.

Therefore, in place of the L1 norm, we propose to compute (and minimize) the L2 norm of the difference between the true transient function  $p(\mathbf{x}_{k+1}|\mathbf{x}_k) = p_{\mathbf{w}_k}(\mathbf{x}_{k+1} - \mathbf{f}_k)$  and its approximation. The L2 norm can be computed in the area  $[-L, L]^{n_x} \times [-\infty, \infty]^{n_x}$  analytically, see Appendix for details. The results for  $n_x = 3$  and  $n_x = 4$  for rectangular and triangular lattices are presented in Tables V and VI, respectively.

Note that the L2 norm of the error can be used for  $n_x = 2$  as well. This leads to the same parameter values as for the L1 norm of the error shown in Table IV.

### H. Gaussian Transient PDF Generally Correlated Elements

Assume now that the process noise is multivariate Gaussian with zero mean and positive definite covariance matrix  $\mathbf{Q}_k$  that is generally time-varying. In that case, we propose a simple linear transformation of the variables in order to convert the problem with  $\mathbf{Q}_k$  equal to the identity matrix.

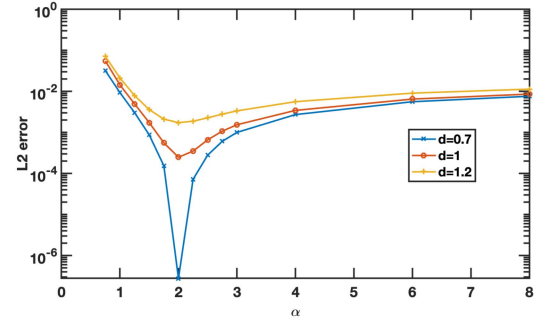


Fig. 6. Fitting error for transients with generalized Gaussian distribution with parameter  $\alpha$ .

Let  $\mathbf{Q}_k = \mathbf{S}_k \mathbf{S}_k^T$  be any matrix  $\mathbf{Q}_k$  decomposition, e.g., the Cholesky decomposition. Define  $\mathbf{x}'_k = \mathbf{S}_k^{-1} \mathbf{x}_k$  and  $\mathbf{f}'_k = \mathbf{S}_k^{-1} \mathbf{f}_k$  for all  $k$ . It can be easily checked that if the PDF of the difference  $\mathbf{x}_{k+1} - \mathbf{f}_k$  is  $\mathcal{N}\{\mathbf{0}, \mathbf{Q}_k\}$ , then the PDF of  $\mathbf{x}'_{k+1} - \mathbf{f}'_k$  is  $\mathcal{N}\{\mathbf{0}, \mathbf{I}\}$ . The modification of the algorithm for arbitrary  $\mathbf{Q}_k$  is thus simple. In each step, the grid points for  $\mathbf{x}_{k+1}$  and  $\mathbf{f}_k$  are normalized, and the CKE is evaluated for the normalized grid points.

### I. Generalized Gaussian Transient PDF

The generalized Gaussian density function with parameter  $\alpha$ , zero mean and variance one is defined as [28].

$$p_\alpha(x) = c_\alpha \exp\{-(\lambda_\alpha |x|)^\alpha\} \quad (27)$$

where  $\alpha > 0$  is a positive parameter that controls the distribution's exponential rate of decay,  $c_\alpha = \frac{\alpha \lambda_\alpha}{2\Gamma(1/\alpha)}$  and  $\lambda_\alpha = \sqrt{\frac{\Gamma(3/\alpha)}{\Gamma(1/\alpha)}}$ , and  $\Gamma(\cdot)$  is the Gamma function. This PDF is a parametric family of distributions that includes both sub-Gaussian distributions (those with kurtosis lower than 3) for  $\alpha > 2$  and super-Gaussian distributions with higher kurtosis and longer tails for  $0 < \alpha < 2$ .

Let the transient PDF have this density,

$$p(x_{k+1}|x_k) = p_\alpha(x_{k+1} - f_k). \quad (28)$$

As in the previous examples, we shall assume that the decomposition (16) holds with the functions  $\mathcal{F}^r$

$$\mathcal{F}^r_{\alpha'}(x) = \beta p_{\alpha'}((x - \mu_r)/\sigma) \quad (29)$$

where  $\beta, \alpha', \sigma$  and  $d$  are parameters to be tuned, and  $d$  is the distance of the neighbor peaks, so that  $\mu_r = rd$ ,  $r = 0, \pm 1, \pm 2, \dots$

Neither L2 nor L1 approximation error is tractable analytically. In this paper, we compute the L2 error by numerical integration of

$$E_2 = \frac{1}{d} \int_{-d/2}^{d/2} \int_{-5}^5 \left[ p_\alpha(x - f) - \sum_{r=-5}^5 \mathcal{F}^r_{\alpha'}(x) \mathcal{F}^r_{\alpha'}(f) \right]^2 dx df.$$

The expression includes five peaks on both sides of point 0. The error is minimized with respect to the parameters  $\beta, \alpha', \sigma$  for given  $d$ ,  $d = 0.7, 1, 1.2$  and given  $\alpha = 0.75, 1, 1.25, \dots, 3, 4, 6, 8$ . The resultant minimum error is shown in Fig. 6. It can be seen that the error is minimum

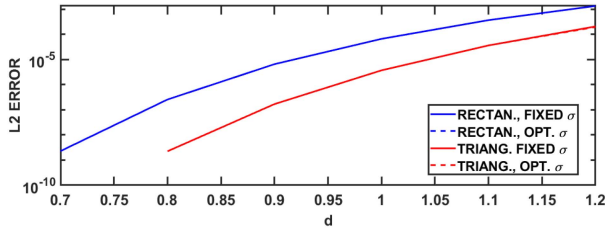


Fig. 7. L2 approximation error of Gaussian transient PDF versus the distance of neighborhood peaks  $d$ . The curves for the optimum  $\sigma$  and for fixed  $\sigma = \sqrt{0.5}$  overlap.

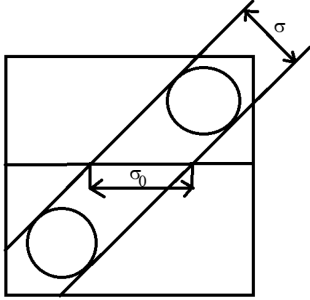


Fig. 8. The square represents the area of the interest, and the diagonal lines mark the width of the transient. The circles stand for the peaks placed along the diagonal to approximate the transient. If  $\sigma_0 = 1$ , then  $\sigma = \sqrt{0.5}$  is the appropriate peak width.

for  $\alpha = 2$ , i.e., for the Gaussian distribution. It follows that the proposed technique with functions  $\mathcal{F}^x$  in the same form as the transient PDF (c.f. (27) and (29)) and may not be suitable for other than Gaussian distributions. In such a case, a more appropriate  $\mathcal{F}^x$  is needed.

### J. Parameter Optimization Aspects

The height  $\beta$  is an element of parameter vector  $\theta$  common to the decompositions of the Gaussian transient PDF (20), (25), Student t-distributed transient PDF (22) and generalized Gaussian transient PDF (29). These decompositions are used in the evaluation of the PMF and mPF weights  $\omega_{k|lm}^{(i)}$  (8). Since the weights are normalized by the constant  $c_{k|lm}$  evaluated using the transient PDF decomposition, the accuracy of the height parameter is unimportant for the filters. In other words, this parameter influences the fitting error of the transient but not the filter itself.

In the case of the Gaussian transient PDF (univariate or multivariate), there is only one other parameter, the width of the peaks, which should be optimized. We can see in Tables I, IV, V, and VI that the optimum width  $\sigma$  is very close to  $\sqrt{0.5} = 0.7071$ , unless the distance  $d$  between the neighborhood peaks is large. For the explanation, see Fig. 8.

In Fig. 7, the L2 approximation error is analyzed for  $n_x = 2$  as a function of parameter  $d$  for (i) the optimum  $\sigma$  and (ii) for fixed  $\sigma = \sqrt{0.5}$ . The difference is negligible; for  $d = 1.2$ , the approximation error for fixed  $\sigma = \sqrt{0.5}$  is  $2.05 \cdot 10^{-4}$  and for the optimum  $\sigma$  the error is  $1.95 \cdot 10^{-4}$ . Their difference is about 5%. Similar results were obtained for  $n_x = 1, 3, 4$  (not shown

here). In conclusion,  $\sigma = \sqrt{0.5}$  and  $\beta = 1$  are good choices in general.

### K. Computational Complexity

In terms of a function evaluation, the standard evaluation of the convolution requires  $\mathcal{O}(N^2)$  evaluations of the transient PDF. The proposed decomposition of the transient PDF then requires  $\mathcal{O}((2N + 1)R)$  evaluations of the function  $\mathcal{F}$ . The proposed decomposition has thus overheads depending on the rank  $R$  (c.f. Fig. 1). For a fixed  $R$ , its computational complexity is linear w.r.t.  $N$ . Thus, for increasing  $N$ , the difference in complexity between the standard evaluation and the proposed one also increases. From the comparison, it follows that the savings due to the decomposition can be expected for  $N \gg R$ .

## IV. NUMERICAL ILLUSTRATION

The performance of the PMF with the proposed transient PDF decomposition is illustrated using terrain-aided navigation (TAN) problem [11] and the univariate non-stationary growth model (UNGM) [29], which is strongly nonlinear and often used as a benchmark problem<sup>9</sup>.

Note that the TAN problem involves a four-dimensional state. A similar TAN problem involving only a two-dimensional state was shown in [19]. For the UNGM, we consider the Student t-distribution of the process to noise to account for its possible outliers.

### A. Terrain-Aided Navigation Problem

Let a state-space model (1), (2) be considered,

$$\mathbf{f}_k(\mathbf{x}_k, \mathbf{u}_k) = \begin{bmatrix} 1 & \frac{\sin(\omega T)}{\omega} & 0 & \frac{1 - \cos(\omega T)}{\omega} \\ 0 & \cos(\omega T) & 0 & -\sin(\omega T) \\ 0 & \frac{1 - \cos(\omega T)}{\omega} & 1 & \frac{\sin(\omega T)}{\omega} \\ 0 & \sin(\omega T) & 0 & \cos(\omega T) \end{bmatrix} \mathbf{x}_k, \quad (30)$$

where  $\mathbf{x}_k = [p_k^N, v_k^N, p_k^E, v_k^E]^T$  is a four-dimensional state vector describing the vehicle horizontal position ( $p_k^N$  and  $p_k^E$ ) and velocity ( $v_k^N$  and  $v_k^E$ ) in north and east directions,  $\omega = 0.02$  rad/s is turn-rate and  $T = 0.2$  s is the sampling period. The equation (30) represents a coordinated turn model (CTM) [30] with a known turn rate, which is independent of the input  $\mathbf{u}_k$ . The state noise density is normal  $p(\mathbf{w}_k) = \mathcal{N}\{\mathbf{w}_k; [0, 0, 0, 0]^T, \mathbf{Q}\}$  with covariance matrix

$$\mathbf{Q} = \begin{bmatrix} \frac{2(\omega T - \sin(\omega T))}{\omega^3} & \frac{1 - \cos(\omega T)}{\omega^2} & 0 & \frac{\omega T - \sin(\omega T)}{\omega^2} \\ \frac{1 - \cos(\omega T)}{\omega^2} & T & \frac{-\omega T + \sin(\omega T)}{\omega^2} & 0 \\ 0 & \frac{-\omega T + \sin(\omega T)}{\omega^2} & \frac{2(\omega T - \sin(\omega T))}{\omega^3} & \frac{1 - \cos(\omega T)}{\omega^2} \\ \frac{\omega T - \sin(\omega T)}{\omega^2} & 0 & \frac{1 - \cos(\omega T)}{\omega^2} & T \end{bmatrix}.$$

The measurement  $z_k$  is the terrain altitude below the vehicle<sup>10</sup> and  $h_k(\cdot)$  denotes a terrain map connecting the sought horizontal position and the available altitude. The measurement noise  $v_k$  includes sensor reading uncertainty and map

<sup>9</sup>Performance of the mPF for the UNGM and TAN ( $n_x = 2$ ) problems has already been analyzed in [20], and thus it is not presented in the manuscript.

<sup>10</sup>Terrain altitude can be based on the barometric altimeter, radar altimeter, or their combination depending on the type of vehicle.

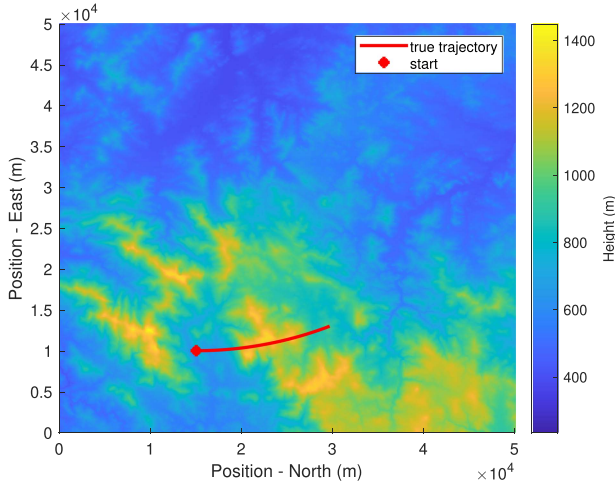


Fig. 9. Simulated trajectory and map.

TABLE VII  
PERFORMANCE EVALUATION FOR THE TAN

	PMF <sub>STD</sub>	PMF <sub>D-rect</sub>	PMF <sub>D-tria</sub>
AAE(pos)	1.488	1.491	1.489
AAE(vel)	0.826	0.870	0.904
$\mathcal{Q}T$ [s]	11 647	2805	2698
RCC	100 %	24.08 %	23.16 %

error. Its pdf is described by  $p(v_k) = \mathcal{N}\{v_k; 0, 2^2\}$ . The system was simulated for 50 time steps with the random initial condition described by Gaussian distribution with mean  $\hat{\mathbf{x}}_0 = [15 \times 10^3 \text{ m}, 750 \text{ m/s}, 10 \times 10^3 \text{ m}, 0 \text{ m/s}]^T$  and covariance matrix  $\mathbf{P}_0 = \text{diag}\{50, 1, 50, 1\}$ . A top-view of the simulated trajectory (start indicated by the circle) and the map are depicted in Fig. 9.

The performance of the following PMF algorithms was analyzed:

- PMF<sub>STD</sub> with the *standard* convolution computation  $N = 30^4 = 81 \times 10^4$ ,
- PMF<sub>D-rect</sub> with the convolution involving the *proposed* transient PDF decomposition with  $N = 30^4$  and rectangular lattice of  $20^4 = 160000$  peaks with parameter  $d = 1$  and corresponding weight and height from Table VI,
- PMF<sub>D-tria</sub> with the convolution involving the *proposed* transient PDF decomposition with  $N = 30^4$  and triangular lattice<sup>11</sup> of 160956 peaks with parameter  $d = 1.2$  and corresponding weight and height from Table VI,

using (i) average absolute error (AAE) of the state estimate for position and velocity, (ii) convolution execution time ( $T$ ), and (iii) relative computational cost saving (RCC). The results can be found in Table VII. They indicate that the average errors in position and velocity of PMF<sub>D-rect</sub> and PMF<sub>D-tria</sub> are comparable to that of PMF<sub>STD</sub>. Also, the computational costs are reduced by more than 75 % by using the decomposition. This reduction would be more pronounced for a higher number of grid points as the complexity of PMF<sub>STD</sub> increases with  $N^2$  whereas the

<sup>11</sup>Note that the parameter  $d$  for the triangular lattice was set to a value larger than for the rectangular lattice to achieve an approximately equal number of peaks for both lattices.

TABLE VIII  
PERFORMANCE EVALUATION FOR THE UNGM

	PMF <sub>ST</sub>	PMF <sub>d(2)</sub>	PMF <sub>d(1.0)</sub>	PMF <sub>d(0.7)</sub>
AMAE	1.3301	1.3717	1.3634	1.3620
$\mathcal{Q}T$ [s]	1.680	0.025	0.043	0.062
RCC	100 %	1.49 %	2.56 %	3.69 %

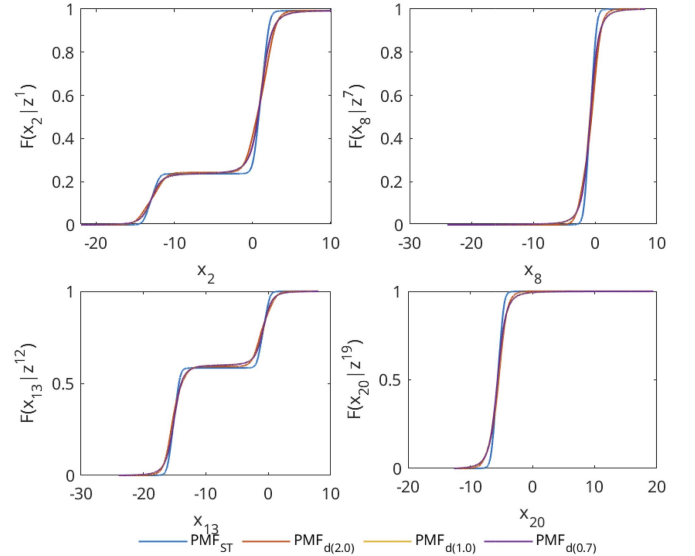


Fig. 10. Comparison of predictive CFD for selected time instants.

complexity of PMF<sub>D</sub>( $\cdot$ ) increases with  $N$  only. Note that in the simulation, we used only 30 points per dimension (i.e.,  $N = 30^4$ ), to keep the PMF<sub>STD</sub> tractable.

### B. UNGM Problem

The model is given by

$$x_{k+1} = 0.5x_k + 25 \frac{x_k}{1+x_k} + 20 \sin(0.05k) + w_k, \quad (31)$$

$$z_k = \frac{x_k^2}{20} + v_k, \quad (32)$$

where  $k = 0, 1, \dots, 30$ , the noise  $w_k$  has Student-t distribution with 3 DoF, the noise  $v_k$  is zero-mean Gaussian with variance  $\text{var}[v_k] = 0.1$ , and the initial state is  $x_0 = 0.1$ . The state was estimated by

- PMF<sub>STD</sub> with the *standard* convolution computation,
- PMF<sub>D(d)</sub> with the convolution involving the *proposed* Student t-distributed transient PDF decomposition with parameter  $d \in \{2, 1.0, 0.7\}$ ,  $L = 20$ , and parameters taken from Table II.

All filters were initialized with  $p(x_0) = \mathcal{N}\{x_0; 0.1, 0.1\}$  and used  $N = 10^4$  grid points.

The model was simulated in  $10^3$  Monte Carlo (MC) simulations. The performance of the filters is analyzed in terms of the average time of the convolution computation ( $T$ ), RCC, and the time average of the mean absolute error (AMAE)

$$\text{AMAE} = \frac{1}{30} \sum_{k=1}^{30} \frac{1}{10^3} \sum_{m=1}^{10^3} |x_k(m) - \hat{x}_k(m)|,$$

where  $x_k(m)$  is the true state at time  $k$  in  $m$ -th MC simulation and  $\hat{x}_k(m)$  is its posterior mean estimate obtained from a PMF. The results are given in Table VIII.

From the table it follows that compared to the algorithm PMF<sub>STD</sub> the algorithms PMF<sub>d(·)</sub> achieve slightly higher AMAE, which decreases with decreasing parameter  $d$ , i.e, increasing rank. The convolution computation time of the PMF<sub>d(·)</sub> is almost by two orders of magnitude lower than that of the PMF with the standard convolution computation. Also, by decreasing the parameter  $d$  (increasing  $R$ ), the computational time is slightly increasing.

Additionally, a comparison of predictive cumulative density functions (CDFs)  $F(x_k|z^{k-1})$  produced by PMF<sub>ST</sub> and PMF<sub>d(·)</sub> for selected time instants is shown in Fig. 10. The results indicate that the PMF algorithms based on the decomposition calculate predictive CDF that is close to the CDF generated by the PMF with the standard convolution. This demonstrates the high quality of the decomposition given the fact that the predictive PDF is multimodal for the challenging UNGM problem.

## V. CONCLUDING REMARKS

The state estimation of nonlinear stochastic dynamic systems by the point-mass filter and marginalized particle filter was treated. The paper proposed a non-negative functional decomposition of the transient density in a closed region, through which the convolution in the filters can efficiently be calculated. The decomposition was particularized for univariate Gaussian, Student t, Cauchy, and multivariate Gaussian transient densities. With a choice of an appropriate rank of the decomposition, significant computational cost savings can be achieved with only negligible loss of filter estimate quality.

An important open problem is how to avoid large ranks of the decomposition, which is significant, especially for higher state dimensions. The problem can be partially addressed by keeping the approximation region small in size. It should be possible in light of the fact that the approximation of the transient density is always affected by only a few components that have peak positions close to the working point. Another open problem is obtaining the decomposition for more general transient densities. It shall however be noted, that the Gaussian and Student t-distributions considered here are the most used distributions of additive process noises in state space models.

## APPENDIX A

### APPENDIX: COMPUTING L2 NORM OF THE ERROR

The Gaussian transient PDF for additive noise in dimension  $n_x$  and its approximation read

$$\begin{aligned} p_{\mathbf{w}_k}(\mathbf{x}_{k+1} - \mathbf{f}_k) &= \frac{1}{(2\pi)^{n_x/2}} \exp\left(-\frac{1}{2}\|\mathbf{x}_{k+1} - \mathbf{f}_k\|^2\right) \\ \hat{p}_{\mathbf{w}_k}(\mathbf{x}_{k+1} - \mathbf{f}_k) &= \sum_{r=1}^R \mathcal{F}(\mathbf{x}_{k+1}; \boldsymbol{\theta}^r) \mathcal{F}(\mathbf{f}_k; \boldsymbol{\theta}^r) \\ &= \sum_{r=1}^R \beta^{n_x} \exp\left(-\frac{\|\mathbf{x}_{k+1} - \boldsymbol{\mu}^r\|^2}{2\sigma^2}\right) \beta^{n_x} \exp\left(-\frac{\|\mathbf{f}_k - \boldsymbol{\mu}^r\|^2}{2\sigma^2}\right) \end{aligned}$$

$$= \beta^{2n_x} \sum_{r=1}^R \exp\left(-\frac{(\|\mathbf{x}_{k+1} - \boldsymbol{\mu}^r\|^2 + \|\mathbf{f}_k - \boldsymbol{\mu}^r\|^2)}{2\sigma^2}\right).$$

In the following, we omit the time indices for convenience and  $\mathbf{x}$ ,  $\mathbf{f}$ , and  $\boldsymbol{\mu}_r$  elements will be denoted  $x_i$ ,  $f_i$ , and  $\mu_i^r$ ,  $i = 1, \dots, n_x$ , respectively. The L2 norm of the error is

$$E = \int_{-L}^L \int_{-\infty}^{\infty} [p_{\mathbf{w}}(\mathbf{x} - \mathbf{f}) - \hat{p}_{\mathbf{w}}(\mathbf{x} - \mathbf{f})]^2 d\mathbf{x} d\mathbf{f}. \quad (33)$$

where

$$d\mathbf{x} d\mathbf{f} = \prod_{i=1}^{n_x} dx_i df_i.$$

The integration with respect to  $x_i$  proceeds from  $-L$  to  $L$  the integration with respect to  $f_i$  proceeds from  $-\infty$  to  $\infty$  for  $i = 1, \dots, n_x$ . For notation simplicity, we shall only use a single integration symbol without explicitly specifying the integration region.

The error is a quadratic function of  $\gamma := \beta^{2n_x}$  so that

$$E = E_1 - 2\gamma E_2 + \gamma^2 E_3, \quad (34)$$

where

$$E_1 = \int p_{\mathbf{w}}(\mathbf{x} - \mathbf{f})^2 d\mathbf{x} d\mathbf{f}, \quad (35)$$

$$E_2 = \frac{1}{\beta^{2n_x}} \int p_{\mathbf{w}}(\mathbf{x} - \mathbf{f}_k) \hat{p}_{\mathbf{w}}(\mathbf{x} - \mathbf{f}) d\mathbf{x} d\mathbf{f}, \quad (36)$$

$$E_3 = \frac{1}{\beta^{4n_x}} \int \hat{p}_{\mathbf{w}}(\mathbf{x} - \mathbf{f})^2 d\mathbf{x} d\mathbf{f} \quad (37)$$

are independent of  $\beta$  ( $\beta$  cancels out) or  $\gamma$ .

Once we have computed the integrals  $E_1$ ,  $E_2$ , and  $E_3$ , the quadratic function in (34) can be minimized with respect to  $\gamma$  in closed form,

$$\gamma_0 = \operatorname{argmin} E(\gamma) = \frac{E_2}{E_3}.$$

Then, the minimum error has the value

$$E(\gamma_0) = E_1 - \frac{E_2^2}{E_3}.$$

The error  $E(\gamma_0)$  is a function of a single scalar parameter  $\sigma$ , which is finally optimized to achieve the minimum error. It holds

$$\begin{aligned} E_1 &= \frac{1}{(2\pi)^{n_x}} \int \exp\left(-\sum_{i=1}^{n_x} (x_i - f_i)^2\right) d\mathbf{x} d\mathbf{f} \\ &= \frac{1}{(2\pi)^{n_x}} \pi^{n_x/2} \int_{-L}^L d\mathbf{f} = \frac{1}{(2\pi)^{n_x}} \pi^{n_x/2} (2L)^{n_x} \\ &= \frac{L^{n_x}}{\pi^{n_x/2}}. \end{aligned} \quad (38)$$

We used the fact that

$$\int_{-\infty}^{\infty} \exp(-t^2) dt = \sqrt{\pi}.$$

Next,

$$E_2 = \frac{1}{(2\pi)^{n_x/2}} \sum_{r=1}^R \int \exp\left(\sum_{i=1}^{n_x} -\frac{(x_i - f_i)^2}{2}\right)$$

$$-\frac{[(x_i - \mu_i^r)^2 + (f_i - \mu_i^r)^2]}{2\sigma^2} d\mathbf{x}d\mathbf{f}. \quad (39)$$

The argument in the sum in (39) can be rewritten as

$$\begin{aligned} & -\frac{(x_i - f_i)^2}{2} - \frac{[(x_i - \mu_i^r)^2 + (f_i - \mu_i^r)^2]}{2\sigma^2} \\ &= -\frac{(x_i - \sigma_1^2(f_i + \frac{\mu_i^r}{\sigma_1^2}))^2}{2\sigma_1^2} - \frac{(f_i - \mu_i^r)^2}{\sigma_2^2} \end{aligned} \quad (40)$$

where

$$\sigma_1 = \sqrt{\frac{\sigma^2}{1 + \sigma^2}} \quad (41)$$

$$\sigma_2 = \sqrt{\frac{2\sigma^2(1 + \sigma^2)}{1 + 2\sigma^2}}. \quad (42)$$

Then,  $E_2$  can be integrated with respect to  $\mathbf{x}$  first to receive

$$\begin{aligned} E_2 &= \frac{\sigma_1^{n_x}}{2^{n_x/2}} \sum_{r=1}^R \int_{-L}^L \exp\left(\sum_{i=1}^{n_x} -\frac{1}{\sigma_2^2}(f_i - \mu_i^r)^2\right) d\mathbf{f} \\ &= \frac{\pi^{n_x/2} \sigma_1^{n_x} \sigma_2^{n_x}}{2^{n_x}} \sum_{r=1}^R \prod_{i=1}^{n_x} \left[ \operatorname{erf}\left(\frac{L - \mu_i^r}{\sigma_2}\right) + \operatorname{erf}\left(\frac{L + \mu_i^r}{\sigma_2}\right) \right] \end{aligned}$$

where  $\operatorname{erf}$  is the error function defined as

$$\operatorname{erf}(x) = \frac{2}{\sqrt{\pi}} \int_0^x \exp(-t^2) dt.$$

Finally,

$$\begin{aligned} E_3 &= \sum_{r=1}^R \sum_{r'=1}^R \int \exp\left(-\frac{1}{2\sigma^2} \sum_{i=1}^{n_x} (x_i - \mu_i^r)^2 + (x_i - \mu_i^{r'})^2 \right. \\ &\quad \left. + (f_i - \mu_i^r)^2 + (f_i - \mu_i^{r'})^2\right) d\mathbf{x}d\mathbf{f} \end{aligned} \quad (43)$$

The argument in the sum in (43) can be rewritten as

$$\begin{aligned} & (x_i - \mu_i^r)^2 + (x_i - \mu_i^{r'})^2 + (f_i - \mu_i^r)^2 + (f_i - \mu_i^{r'})^2 \\ &= \left(x_i - \frac{\mu_i^r + \mu_i^{r'}}{2}\right)^2 + \left(f_i - \frac{\mu_i^r + \mu_i^{r'}}{2}\right)^2 + (\mu_i^r - \mu_i^{r'})^2. \end{aligned} \quad (44)$$

The resultant expression is

$$\begin{aligned} E_3 &= \frac{\pi^{n_x} \sigma^{2n_x}}{2^{n_x}} \sum_{r=1}^R \sum_{r'=1}^R \prod_{i=1}^{n_x} \exp\left(-(\mu_i^r - \mu_i^{r'})^2\right) \\ &\quad \left[ \operatorname{erf}\left(\frac{L - \frac{(\mu_i^r + \mu_i^{r'})}{2}}{\sigma}\right) + \operatorname{erf}\left(\frac{L + \frac{(\mu_i^r + \mu_i^{r'})}{2}}{\sigma}\right) \right]. \end{aligned} \quad (45)$$

## REFERENCES

- [1] A. Doucet, N. De Freitas, and N. Gordon, *Sequential Monte Carlo Methods in Practice*. Berlin, Germany: Springer, 2001.
- [2] F. Gustafsson, "Particle filter theory and practice with positioning applications," *IEEE Aerosp. Electron. Syst. Mag.*, vol. 25, no. 7, pp. 53–82, Jul. 2010.
- [3] M. Šimandl, J. Královec, and T. Söderström, "Anticipative grid design in point-mass approach to nonlinear state estimation," *IEEE Trans. Autom. Control*, vol. 47, no. 4, pp. 699–702, Apr. 2002.
- [4] H. W. Sorenson, "On the development of practical nonlinear filters," *Inf. Sci.*, vol. 7, pp. 230–270, 1974.
- [5] M. Šimandl, J. Královec, and T. Söderström, "Advanced point-mass method for nonlinear state estimation," *Automatica*, vol. 42, no. 7, pp. 1133–1145, 2006.
- [6] J. Matoušek, J. Duník, and O. Straka, "Point-mass filter: Density specific grid design and implementation," in *Proc. 15th Eur. Workshop Adv. Control Diagnosis*, 2019, pp. 1093–1115.
- [7] M. Klaas, N. de Freitas, and A. Doucet, "Toward practical N2 Monte Carlo: The marginal particle filter," 2012, *arXiv:1207.1396*.
- [8] V. Šmídl and M. Gašperin, "Rao-blackwellized point mass filter for reliable state estimation," in *Proc. IEEE 16th Int. Conf. Inf. Fusion*, 2013, pp. 312–318.
- [9] J. Duník, M. Soták, M. Veselý, O. Straka, and W. J. Hawkinson, "Design of Rao-Blackwellised point-mass filter with application in terrain aided navigation," *IEEE Trans. Aerosp. Electron. Syst.*, vol. 55, no. 1, pp. 251–272, Feb. 2019.
- [10] J. N. Lim and C. G. Park, "RBPPFF for robust TAN," *IET Radar, Sonar Navigation*, vol. 13, no. 12, pp. 2230–2243, 2019.
- [11] N. Bergman, "Recursive Bayesian estimation: Navigation and tracking applications," *Ph.D. dissertation*, Linköping University, Linköping, Sweden, 1999.
- [12] J. Duník, O. Straka, J. Matoušek, and E. Blasch, "Copula-based convolution for fast point-mass prediction," *Signal Process.*, vol. 192, 2022, Art. no. 108367.
- [13] C. Kalender and A. Schottl, "Sparse grid-based nonlinear filtering," *IEEE Trans. Aerosp. Electron. Syst.*, vol. 49, no. 4, pp. 2386–2396, Oct. 2013.
- [14] M. Klaas, M. Briens, N. de Freitas, A. Doucet, S. Maskell, and D. Lang, "Fast particle smoothing: If I had a million particles," in *Proc. 23rd Int. Conf. Mach. Learn.*, 2006, pp. 481–488.
- [15] F. Gustafsson, "On marginal particle filters with linear complexity," in *Proc. IEEE 5th Int. Workshop Comput. Adv. Multi-Sensor Adaptive Process.*, 2013, pp. 356–359.
- [16] Ji-Cheng Chen, "The nonnegative rank factorizations of nonnegative matrices," *Linear Algebra its Appl.*, vol. 62, pp. 207–217, 1984.
- [17] P. Paatero and U. Tapper, "Positive matrix factorization: A non-negative factor model with optimal utilization of error estimates of data values," *Environmetrics*, vol. 5, no. 2, pp. 111–126, 1994.
- [18] K. Huang, N. D. Sidiropoulos, and A. Swami, "Non-negative matrix factorization revisited: Uniqueness and algorithm for symmetric decomposition," *IEEE Trans. Signal Process.*, vol. 62, no. 1, pp. 211–224, Jan. 2014.
- [19] P. Tichavský, O. Straka, and J. Duník, "Point-mass filter with decomposition of transition density," in *Proc. IEEE Int. Conf. Acoust., Speech and Signal Process.*, 2022, pp. 5752–5756.
- [20] O. Straka and J. Duník, "Efficient implementation of marginal particle filter by functional density decomposition," in *Proc. IEEE 25th Int. Conf. Inf. Fusion*, 2022, pp. 01–08.
- [21] B. Ristic, S. Arulampalam, and N. Gordon, *Beyond the Kalman Filter: Particle Filters for Tracking Applications*, Norwood, MA, USA: Artech House, 2004.
- [22] B. D. O. Anderson and J. B. Moore, *Optimal Filtering*. Hoboken, NJ, USA: Prentice Hall, 1979.
- [23] A. A. Gorodetsky, S. Karaman, and Y. M. Marzouk, "A continuous analogue of the tensor-train decomposition," *Comput. Methods Applied Mechanics and Eng.*, vol. 347, pp. 59–84, 2019.
- [24] M. Roth, E. Özkan, and F. Gustafsson, "A student's-t filter for heavy tailed process and measurement noise," in *Proc. IEEE Int. Conf. Acoust., Speech and Signal Process.*, 2013, pp. 5770–5774.
- [25] Jeffrey C. Lagarias, James A. Reeds, Margaret H. Wright, and Paul E. Wright, "Convergence properties of the nelder-meade simplex method in low dimensions," *SIAM J. Optim.*, vol. 9, no. 1, pp. 112–147, 1998.
- [26] G. Kitagawa, "Non-gaussian state-space modeling of nonstationary time series," *J. Amer. Stat. Assoc.*, vol. 82, no. 400, pp. 1032–1041, 1987.
- [27] K. Critchlow, *Order in Space: A Design Source Book*. London, U.K.: Thames and Hudson, 1976.
- [28] Mahesh K. Varanasi and B. Aazhang, "Parametric generalized Gaussian density estimation," *J. Acoust. Soc. America*, vol. 86, no. 4, pp. 1404–1415, 1989.
- [29] N. Gordon, D. Salmund, and A. F. M. Smith, "Novel approach to nonlinear/non-Gaussian Bayesian state estimation," *IEE Proc.-F*, pp. 107–113, 1993.
- [30] F. Gustafsson and A. J. Isaksson, "Best choice of coordinate system for tracking coordinated turns," in *Proc. IEEE 35th Conf. Decis. Control*, 1996, pp. 3145–3150.



**Petr Tichavský** (Senior Member, IEEE) received the Ph.D. degree and the Research Professor (DSc.) degree in theoretical cybernetics from the Czech Academy of Sciences, Prague, Czech Republic, in 1992 and 2017, respectively.

He is currently with the Institute of Information Theory and Automation, Czech Academy of Sciences, Prague. He is the author or coauthor of research articles in the area of sinusoidal frequency/frequency-rate estimation, adaptive filtering and tracking of time-varying signal parameters,

algorithm-independent bounds on achievable performance, sensor array processing, independent component analysis, blind source separation, and tensor decompositions.

Dr. Tichavský has been a member of the IEEE SPS Committee Signal Processing Theory and Methods from 2008 to 2011 and from 2016 to 2019. He was also the General Co-Chair of the 36th IEEE International Conference on Acoustics, Speech, and Signal Processing ICASSP 2011 in Prague. He served as an Associate Editor for the IEEE SIGNAL PROCESSING LETTERS from 2002 to 2004 and as an Associate Editor for the IEEE TRANSACTIONS ON SIGNAL PROCESSING from 2005 to 2009 and from 2011 to 2016.



**Ondřej Straka** (Member, IEEE) received the master's degree in cybernetics and control engineering and the Ph.D. degree in cybernetics from the University of West Bohemia, Pilsen, Czech Republic, in 1998 and 2004, respectively. Since 2015, he has been an Associate Professor with the Department of Cybernetics, University of West Bohemia. He is the Head of the Identification and Decision Making Research Group (IDM), NTIS-New Technologies for the Information Society. He has participated in a number of projects of fundamental and applied research. He

was involved in development of several software frameworks for nonlinear state estimation and system identification. He has co-authored over 140 journal and conference papers in journals. His current research interests include local and global nonlinear state estimation methods, system identification, performance evaluation, and fault detection.

Dr. Straka was a recipient of Werner von Siemens Excellence Award in 2014 for most important result in the basic research.



**Jindřich Duňík** (Senior Member, IEEE) received Ing. (M.Sc.) and Ph.D. degrees in automatic control in 2003 and 2008, respectively, both from the University of West Bohemia (UWB), Pilsen, Czech Republic. He is an associate professor at the Department of Cybernetics, UWB, focusing on state estimation and system identification, and a senior scientist with Honeywell International, Aerospace Advanced Technology Europe (ATE), working in inertial and satellite-based navigation systems and integrity monitoring methods. He has authored or co-authored more than 80

technical papers (both journal and conference) and patents devoted to nonlinear filtering, system identification, and navigation. He is an associate editor for the special issue on Machine Learning Methods for Aerial and Space Positioning Navigation in IEEE TRANSACTIONS ON AEROSPACE AND ELECTRONIC SYSTEMS and has served as a member of technical committees at several conferences. He received Honeywell Technology Achievement Awards, Werner von Siemens Excellence Award, and IEEE AESS Harry Rowe Mimno Award.